Talanta 87 (2011) 243–248

Contents lists available at SciVerse ScienceDirect

Talanta

journal homepage: www.elsevier.com/locate/talanta

An amperometric hydrogen peroxide chemical sensor based on graphene-Fe_3O_4 multilayer films modified ITO electrode

Xuexia Liu[a,b], Hui Zhu[a], Xiurong Yang[a,b,*]

[a] State Key Laboratory of Electroanalytical Chemistry, Changchun Institute of Applied Chemistry, Chinese Academy of Sciences, Changchun, Jilin 130022, China
[b] Graduate School of the Chinese Academy of Sciences, Beijing 100039, China

ARTICLE INFO

Article history:
Received 29 July 2011
Received in revised form
29 September 2011
Accepted 4 October 2011
Available online 10 October 2011

Keywords:
$(PDDA\text{-}G/Fe_3O_4)_n$ multilayer films
Hydrogen peroxide chemical sensor
Layer-by-layer assembly

ABSTRACT

In this article, poly(diallydimethylammonium chloride) (PDDA) functionalized graphene-Fe_3O_4 (PDDA-G/Fe_3O_4)$_n$ multilayer films were fabricated with layer-by-layer assembly of negatively charged Fe_3O_4 nanoparticles (Fe_3O_4 NPs) and positively charged PDDA-G through the electrostatic interaction to construct a H_2O_2 chemical sensor. The multilayer films were characterized with UV–vis spectroscopy, atomic force microscopy and cyclic voltammetry. The participation of PDDA-G improved the catalytic ability of Fe_3O_4 NPs due to its high surface area and excellent electric conductivity. Based on this, the obtained H_2O_2 chemical sensor exhibited prominent electrocatalytic activity for the detection of H_2O_2 with a wide linear range from 20 μM to 6.25 mM, a rapid response upon the addition of H_2O_2 and a low detection limit of 2.5 μM with the signal to noise ratio of three. Furthermore, the fabricated nonenzymatic H_2O_2 chemical sensor exhibited excellent stability and reproducibility.

1. Introduction

Graphene, a one-atom-thick two-dimensional structure of sp^2-bonded carbon, has inspired great enthusiasm since its discovery by Geim and Novoselov in 2004 [1]. Due to its unique properties including strong mechanical strength, large specific surface area, high charge-carrier mobility and excellent electric conductivity [2,3], graphene has found great application potential in many fields, such as energy storage materials [4,5], nanoelectronics [6,7], polymer composite materials [8,9] and electrochemical sensor [10,11]. In addition, compared with the commonly used carbon nanotubes (CNTs), graphene exhibits potential advantages of low cost, ease of processing and safety [12]. Graphene can be prepared by mechanical cleavage [1], chemical vapor deposition (CVD) [13], solvent thermal reaction [14], epitaxial growth on silicon carbide [15] and direct chemical reduction of graphene oxide (GO) [16,17]. Due to its versatility and scale up, the chemical reduction of GO is considered as one of the most attractive approaches to prepare graphene sheets. Up to now, many kinds of reducing species have been explored [9,16,17]. However in most cases, a large amount of protecting agents function as barriers to prevent the reduced graphene from aggregation [8,17,18]. Recently, Lin and co-workers prepared well-dispersed graphene suspension using PDDA as a reducing agent [19]. The exposed surface of graphene provides good support for the electroactive materials and facilitates the mass transportation [20]. In addition, the layer-by-layer assembly approach is widely used to fabricate hybrid multilayer films with excellent properties. For example, Ye's group fabricated multilayer films using layer-by-layer assembled graphene modified with polyelectrolytes by covalent binding [21]. Zhu et al. constructed multilayer films by alternatively assembling positively charged graphene nanosheets and negatively charged Pt nanoparticles [22]. Therefore, it is reasonable to believe that layer-by-layer assembly is a promising approach to construct graphene-based nanocomposites.

Magnetic nanoparticles have enormous applications in electronic devices, magnetic data storage, drug delivery and magnetic resonance [23]. More importantly, Fe_3O_4 nanoparticles (Fe_3O_4 NPs) possess an intrinsic enzyme mimetic activity like natural peroxidases [24]. The rapid and accurate determination of hydrogen peroxide (H_2O_2) is of significant importance in many fields including medicine, food industry, biology and environmental protection [25]. Besides, H_2O_2 is a byproduct of several highly selective oxidases. Conventional techniques employed for the determination of H_2O_2 such as UV–vis spectrophotometry [26], titrimetry [27] and electrochemical method based on enzyme modified electrodes [28,29] have been reported in literatures. Enzyme-based method is considered as one of the most attractive approaches to detect H_2O_2. For example, Zhu and co-workers prepared graphene-Fe_3O_4 composites with a solvothermal method for the immobilization of horseradish peroxidase to construct a H_2O_2 biosensor [30]. Zheng and co-workers constructed an amperometric H_2O_2 sensor based

* Corresponding author at: State Key Laboratory of Electroanalytical Chemistry, Changchun Institute of Applied Chemistry, Chinese Academy of Sciences, Changchun, Jilin 130022, China. Tel.: +86 0431 85262056; fax: +86 0431 85689278.
E-mail address: xryang@ciac.jl.cn (X. Yang).

0039-9140/$ – see front matter © 2011 Elsevier B.V. All rights reserved.
doi:10.1016/j.talanta.2011.10.004

on the immobilization of hemoglobin on the magnetite-graphene modified carbon ceramic electrode [28]. However, there are several disadvantages of electrochemical method based on enzyme modified electrodes, such as high cost of enzymes, susceptibility to temperature and pH value, inherent instability and complicated immobilization procedure. Therefore, the development of nonenzyme composites modified and highly sensitive sensor is especially promising to overcome these shortcomings.

In this article, the Fe_3O_4 NPs were used as excellent substitutes for peroxidase enzymes. We fabricated poly(diallydimethylammonium chloride) (PDDA) functionalized graphene-Fe_3O_4 (PDDA-G/Fe_3O_4)$_n$ multilayer films on indium tin oxide (ITO) substrate through electrostatic interaction by means of the layer-by-layer assembly method (shown in Fig. 1). The electrochemical reduction behavior of H_2O_2 was investigated. The modified electrode showed a fast response on H_2O_2, a wide linear range and a low detection limit towards H_2O_2. In addition, the fabricated nonenzymatic H_2O_2 sensor exhibited excellent stability and reproducibility.

2. Experimental

2.1. Reagents

Nature graphite was purchased from Alfa Aesar. PDDA (Mw 200–350 kg/mol, 20 wt% aqueous solution) and tetramethylammonium hydroxide (TMAOH) were obtained from Sigma-Aldrich. Potassium persulfate was purchased from Acros. Potassium permanganate ($KMnO_4$), ferric chloride hexahydrate, iron (II) sulfate heptahydrate, 98% H_2SO_4, 30% H_2O_2, 25% $NH_3{\cdot}H_2O$ and 36% HCl were obtained from Beijing Chemical Reagent Factory. All reagents were of analytical grade and used as received without further purification. Double-distilled (DI) water from a Millipore system (>18 MΩ cm) was employed throughout the experiment.

2.2. Apparatus

Transmission electron microscopy (TEM) was carried out with JEM-2000 FX operating at 200 kV accelerating voltage and atomic force microscopy (AFM) measurements were made on the mica or quartz with Veeco Instruments Nanoscope in tapping mode. X-ray photoelectron spectroscopy (XPS) measurements were performed on an ESCALAB MK II photoelectron spectrometer (VG Co., UK) with Al Kα X-ray radiation as the X-ray source for excitation. UV–visible (UV–vis) spectra were recorded on a Cary 50 UV–vis spectrophotometer. Electrochemical measurements were carried out with a CHI 660B electrochemical station (Shanghai, China). In the three-electrode system, the (PDDA-G/Fe_3O_4)$_n$ multilayer films modified ITO electrode was selected as a working electrode, Ag/AgCl (saturated potassium chloride) was chosen as a reference electrode, and a platinum foil was employed as a counter electrode.

2.3. Synthesis of PDDA-G and Fe_3O_4 NPs

GO was synthesized by a modified Hummers method [18,31,32]. GO was reduced to PDDA-G using PDDA according to the previous report [19]. In brief, 100 mL of GO (0.99 mg/mL) solution was mixed with 6 mL PDDA (20 wt%) solution under vigorous stirring for 10 min. Then the mixture was heated to 90 °C and maintained for 5 h in refluxing conditions. The color of the solution changed from yellow-brown to black gradually, indicating the formation of PDDA-G. The resulting product was cooled to room temperature and washed with DI water via centrifugation. The obtained PDDA-G was dispersed into 40 mL DI water with the concentration of 3.39 mg/mL.

Fe_3O_4 NPs were synthesized according to Massart's method [33]. Under vigorous stirring, 12.5 mL freshly prepared aqueous mixture of ferric chloride (10 mL, 1 M) and ferrous sulfate (2.5 mL, 2 M, in HCl 2 M) was added to ammonia solution (125 mL, 0.7 M). After 30 min the precipitate was collected on the vessel wall by a permanent magnet and the clear supernatant was decanted. The obtained product was redispersed in DI water and TMAOH (1 M) was added with vigorous stirring.

2.4. Synthesis of (PDDA-G/Fe_3O_4)$_n$ multilayer films

ITO wafers were cleaned by sonicating in acetone, ethanol and DI water separately for 20 min and rinsed with copious amounts of DI water and then dried with nitrogen. The multilayer films were prepared by alternatively immersing the ITO into positively charged PDDA-G and negatively charged Fe_3O_4 NPs solutions for 20 min separately until the desired number of layers was achieved. ITO was washed with DI water and dried with nitrogen after each dipping step. For UV–vis absorption and AFM analysis, multilayer films were also prepared on the quartz wafers. Quartz wafers were cleaned by soaking in slightly boiled piranha solution (35 mL, 98% H_2SO_4 and 15 mL, 30% H_2O_2) for 40 min and then rinsed with plenty of DI water (*Caution: piranha solution reacts violently with organic materials and should be handled carefully*). Successively, quartz wafers were dried with nitrogen stream.

3. Results and discussion

3.1. Characterization of GO and PDDA-G

Fig. 2 depicts the XPS spectra of GO and PDDA-G. As shown in Fig. 2A and D, a new peak corresponding to the nitrogen element was identified in the PDDA-G sample, which confirmed the strong interaction between PDDA molecules and graphene scaffold. In addition, the spectra of C 1s peak (Fig. 2B and C) could be deconvoluted into five components arising from carbonyl carbon (C=O, 288.1 eV), epoxy carbon (286.6 eV), C–O (285.4 eV) and non-oxygenated carbon (284.3 eV), indicating a high content of oxygen in graphene oxide [34]. However, the intensities of oxygen related peaks decreased with the appearance of C–N bond (285.9 eV) in Fig. 2C [35]. The calculated oxygen content reduced from 27.5% to 17.5%. These phenomena verified the effective reduction and successful decoration of PDDA to graphene, accordant with the color variation from yellow-brown to black. Furthermore, the resulted GO and PDDA-G were also characterized by AFM (Fig. 3). As measured from the height profile, the average thickness of PDDA-G was about 1.2 nm and the obtained GO sheet was only about 0.86 nm (less than 1 nm) [36]. Compared with the normal reported thickness of single-sheet graphene (less than 0.9 nm) [16,37], the thickness of the PDDA-G is larger. This thickness increase might arise from the effective adsorption of PDDA onto graphene frameworks via the π–π interaction [19]. The obtained PDDA-G was also characterized by zeta potential to study the charge state. Conventional graphene preserves residual defect with negatively charges, such as carboxyl, hydroxyl and epoxy groups [38]. On the contrary, the obtained PDDA-G showed a positive zeta potential (54.7 mV) after reduction by PDDA, indicating that the graphene was successfully functionalized by the positively charged PDDA. Thus, it is reasonable to conclude that PDDA plays an important role in reduction and decoration of graphene.

3.2. Characterization of Fe_3O_4 NPs

Fe_3O_4 NPs were prepared according to Massart's method [33]. As shown in the TEM image of Fe_3O_4 NPs (Fig. S1), the size distribution of the obtained magnetic nanoparticles was about 6–10 nm.

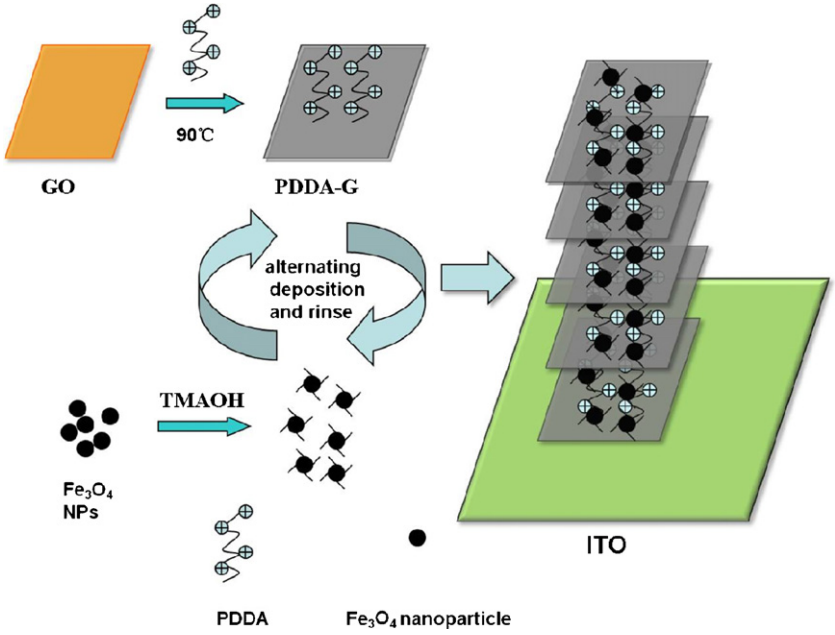

Fig. 1. Scheme illustrating the formation of $(PDDA\text{-}G/Fe_3O_4)_n$ multilayer films through electrostatic interaction.

Moreover, TMAOH was a popular stabilizer for preparation of Fe_3O_4 NPs. The formation of double electric layer endowed Fe_3O_4 NPs with negative charges in the basic medium. The positively charged tetramethylammonium acted as counter ion here [39]. The zeta potential of TMAOH stabilized Fe_3O_4 NPs was −37.9 mV. Therefore, we may conclude that negatively charged Fe_3O_4 NPs could be easily assembled with positively charged PDDA-G through electrostatic interaction.

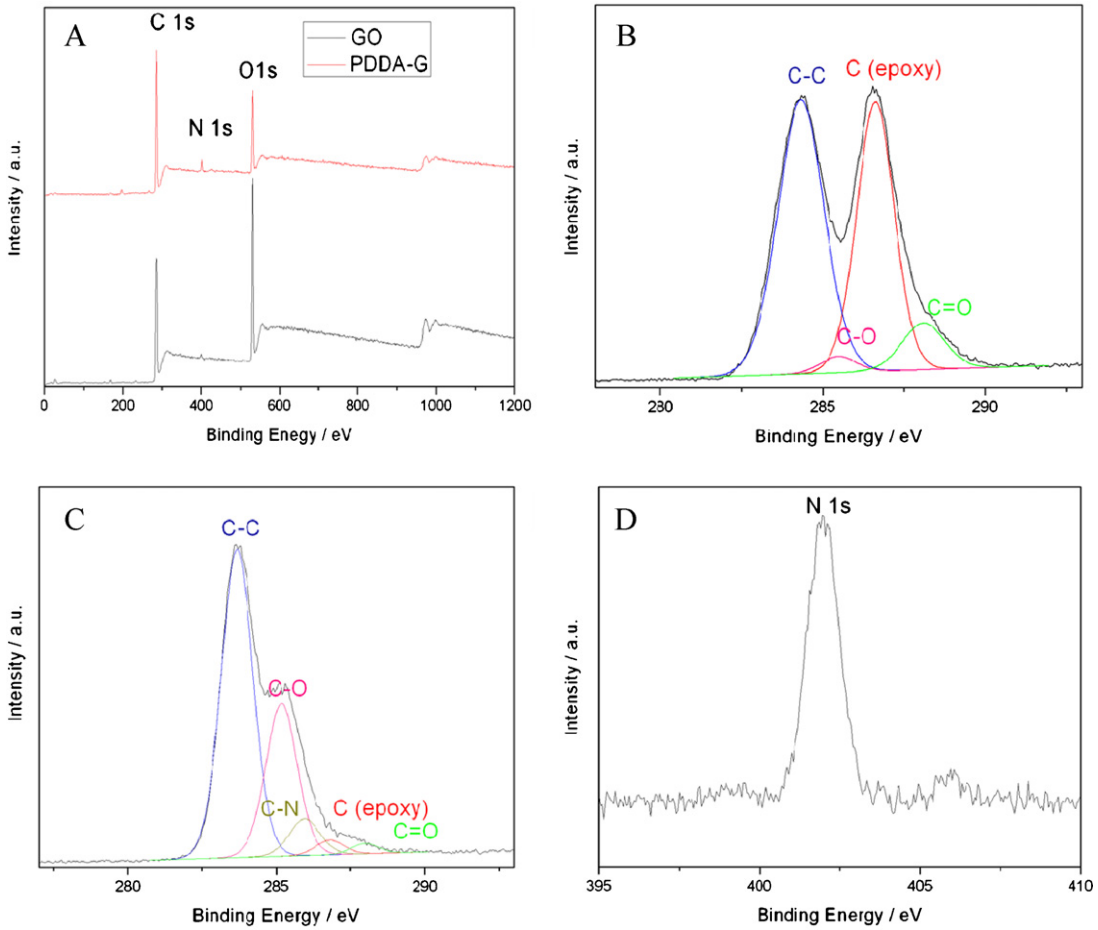

Fig. 2. XPS spectra of (A) GO and PDDA-G, (B) C 1s in GO, (C) C 1s in PDDA-G, (D) N 1s in PDDA-G.

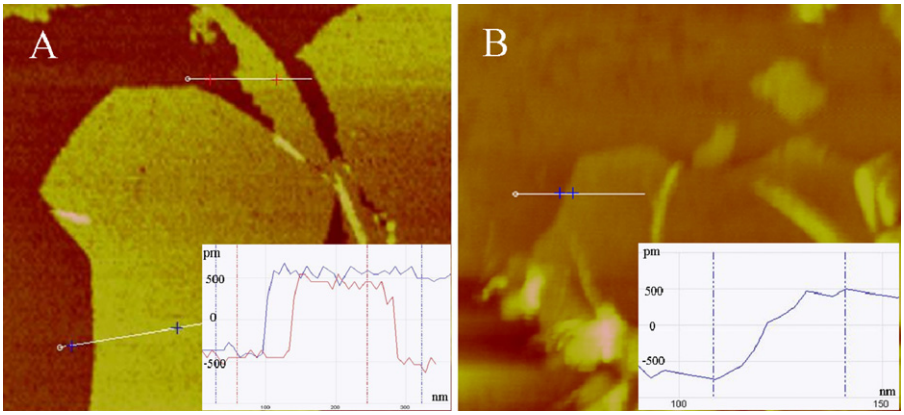

Fig. 3. AFM images of (A) GO and (B) PDDA-G on mica through drop-casting.

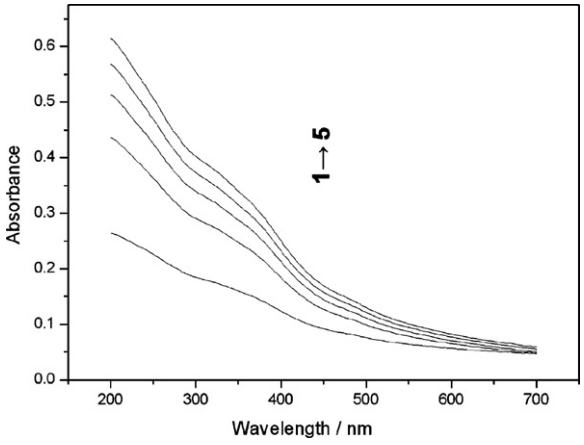

Fig. 4. UV–vis absorption spectra of layer-by-layer assembled $(PDDA\text{-}G/Fe_3O_4)_n$ multilayer films on quartz glass substrate with different number of bilayers: 1–5.

3.3. Characterization of $(PDDA\text{-}G/Fe_3O_4)_n$ multilayer films

Based on the data above, positively charged PDDA-G and negatively charged Fe_3O_4 NPs were layer-by-layer assembled through electrostatic interaction. Fig. 4 displays the UV–vis absorption spectra of $(PDDA\text{-}G/Fe_3O_4)_n$ multilayer films (with $n = 1–5$) assembled on the quartz substrate. The absorbance of the films increased with the increase of bilayer number, indicating the successful fabrication of multilayer films. Furthermore, morphological characterization was conducted via AFM images. As displayed in Fig. 5A, different from the random dispersion on the quartz substrate, most of the Fe_3O_4 NPs aggregated on the PDDA-G sheets. This might result from the electrostatic interaction between them. The outline of the PDDA-G could still be seen. When 5 bilayers were assembled on the substrate, the film became much thicker and a large amount of Fe_3O_4 NPs were adsorbed compactly on PDDA-G sheets (Fig. 5B) [22]. Both of these characterizations proved the successful assembly of PDDA-G and Fe_3O_4 NPs.

3.4. $(PDDA\text{-}G/Fe_3O_4)_n$ multilayer films modified ITO electrode for H_2O_2 detection

The bare ITO electrode has only a small current response to H_2O_2 (Fig. 6) [40]. If it was decorated with Fe_3O_4 NPs, the reduction current increased to a certain extent. However, due to the magnetic interaction, Fe_3O_4 NPs always aggregated seriously, hindering the mass transfer on the electrode surface. Graphene has large specific surface area, high charge-carrier mobility and excellent electric conductivity [2,3]. It was found the fact that integrating graphene with metal or metal oxide nanoparticles exhibited enhanced electrocatalytic activity [19,41]. Therefore, $(PDDA\text{-}G/Fe_3O_4)_n$ multilayer modified electrode with promoted electrocatalytical ability towards H_2O_2 was envisioned. The effect of bilayer number to the result was investigated. The differences of the current response of different bilayer number were minor (Fig. S2). For a typical sample, we investigated the electrocatalytic

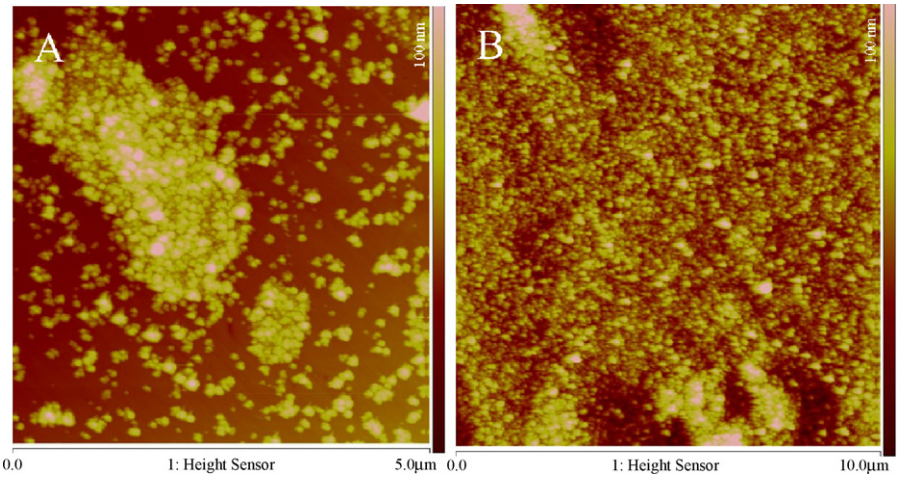

Fig. 5. AFM images of the (A) $(PDDA\text{-}G/Fe_3O_4)_1$ and (B) $(PDDA\text{-}G/Fe_3O_4)_5$ multilayer films on the quartz glass substrate.

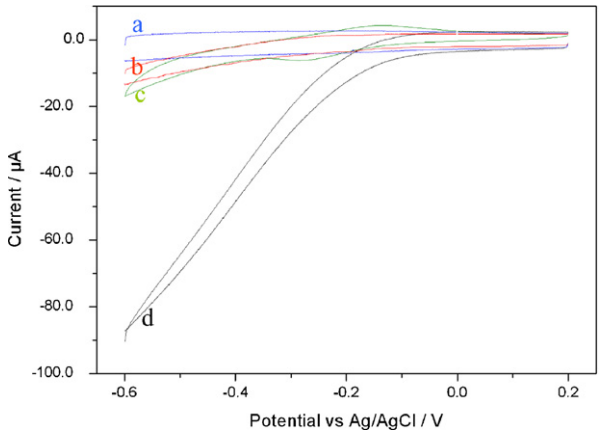

Fig. 6. Cyclic voltammograms of bare ITO (a, b) and $(PDDA\text{-}G/Fe_3O_4)_5$ multilayer films (c, d) modified ITO electrode in the absence (a, c) and presence (b, d) of 1.5 mM H_2O_2 in PBS (0.1 M, pH 7.0) with air saturated at the scan rate 100 mV/s.

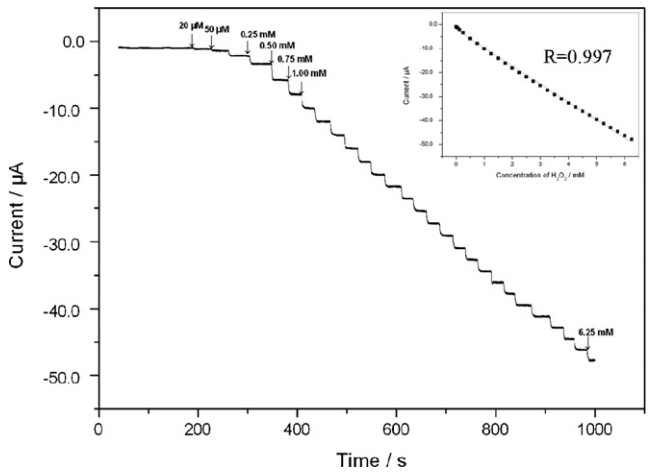

Fig. 7. Typical amperometric current response of the $(PDDA\text{-}G/Fe_3O_4)_5$ multilayer films modified electrode on the successive injection of H_2O_2 with various concentrations into stirring PBS (0.1 M, pH 7.0). Inset: calibration curve of H_2O_2 concentration on the modified electrode.

activity of the $(PDDA\text{-}G/Fe_3O_4)_5$ multilayer films. Fig. 6 shows the cyclic voltammograms (CVs) of the $(PDDA\text{-}G/Fe_3O_4)_5$ multilayer films modified ITO electrode in the absence (curve *c*) and presence of 1.5 mM H_2O_2 (curve *d*) in PBS (0.1 M, pH 7.0) with air saturated at a scan rate of 100 mV/s. Compared with the bare ITO electrode (curve *a* and *b*), the reduction current showed a great increase when H_2O_2 was introduced into CVs measurement experiment, indicating that $(PDDA\text{-}G/Fe_3O_4)_5$ multilayer films possessed efficient electrocatalytical activity towards H_2O_2. The other distinctive feature is that our experiment can be conducted without the saturation of N_2 as reported by others [40,42]. To check the effect of N_2, cyclic voltammograms experiments with N_2 saturated were also performed, the curve response to H_2O_2 was almost the same as that performed with air saturated (Fig. S3), indicating that the effect of N_2 could be neglected in our work. Therefore, $(PDDA\text{-}G/Fe_3O_4)_5$ multilayer films could efficiently electrocatalyze the reduction of H_2O_2 with air saturated environment.

Considering the sensitivity and stability, −0.4 V was selected as an applied potential for amperometric experiment. Fig. 7 displays a typical current–time plot of $(PDDA\text{-}G/Fe_3O_4)_5$ multilayer modified electrode on the successive addition of H_2O_2 with various concentrations into stirring PBS (0.1 M, pH 7.0) at the applied potential of −0.4 V. A rapid current response could be observed when H_2O_2 was added to the solution. The maximum steady-state current could be achieved within 4.5 s, indicating a fast H_2O_2 diffusion process in the modified electrode due to the porous structure of the film as demonstrated in AFM [40]. The current response increased linearly with the concentration of H_2O_2. The inset of Fig. 7 shows the calibration curve between the response current and the concentration of H_2O_2. The electrode had a wide linear range from 20 μM to 6.25 mM with a correlation coefficient of 0.997, which was much wider than some reported biosensors based on horseradish peroxidase (please see Table 1) [30,43,44]. The detection limit of this electrode was estimated to be 2.5 μM with the signal to noise ratio of three. The absorbance of the $(PDDA\text{-}G/Fe_3O_4)_5$ multilayer films was much weaker than $(PDDA/Fe_3O_4)_5$ multilayer films on quartz substrate, indicating that the content of Fe_3O_4 NPs in our film was lower than the reported $(PDDA/Fe_3O_4)_5$ multilayer films [40]. However, the current response was similar to the reported literature. These results demonstrated that the participation of PDDA-G facilitated the reaction between the electrode and Fe_3O_4 NPs and thus improved the catalytic ability of Fe_3O_4 NPs.

3.5. Stability, reproducibility and interferences of the $(PDDA\text{-}G/Fe_3O_4)_5$ multilayer film modified electrode

The reproducibility of the $(PDDA\text{-}G/Fe_3O_4)_5$ multilayer modified ITO electrode was investigated by measuring the current response of the electrode on 1 mM H_2O_2 in PBS (0.1 M, pH 7.0). The relative standard deviation (RSD) of the current response was 3.4% for 6 successive determinations of 1 mM H_2O_2. To evaluate the stability of the modified electrode, the current response to H_2O_2 was examined at the same condition. The current signal decreased 8% after two weeks. The most common interferents for H_2O_2 during the electrochemical measurement include ascorbic acid, citric and cysteine. As shown in the inset of Fig. S3, the current response almost did not change after addition of ascorbic, and the current responses changed about −18% for citric and cysteine, indicating that both citric and cysteine had neglectable influence on the H_2O_2 detection. These results revealed that $(PDDA\text{-}G/Fe_3O_4)_5$ multilayer modified ITO electrode could be satisfactory for H_2O_2 determination with good reproducibility and stability.

3.6. Real sample determination

The prepared chemical sensor was applied for determination of H_2O_2 in commercial toothpaste and standard addition method was used in sample analysis procedure. As shown in Table 2, the results were compared with those determined by classical potassium permanganate titration method [45]. In brief, 1 g of toothpaste was dissolved into 50 mL PBS, which was respectively titrated with 0.01 M potassium permanganate standard solution and determined

Table 1
Comparison of the performance of various H_2O_2 sensors.

Materials	Sensitivity ($\mu A\,mM^{-1}\,cm^{-2}$)	Linear range (mM)	Detection limit (μM)	Reference
$PDDA/Fe_3O_4$	–	0.00418–0.8	1.4	[40]
HPP/CHIT/CMS/GS	120.17	0.1–1.6	0.93	[43]
HRP	12.8	0.004–0.1	1.6	[44]
$G\text{-}Fe_3O_4/CH/HRP$	132	0.005–3.81	0.6	[30]
$PDDA\text{-}G/Fe_3O_4$	61.2	0.02–6.25	2.5	This work

Table 2
Concentrations of H_2O_2 in real samples determined by the $(PDDA\text{-}G/Fe_3O_4)_5$ chemical sensor and the classical titration method.

Experiment no.	Concentrations of H_2O_2 in toothpaste ($\mu g\,g^{-1}$)			Relative error[a] (%)
	Sensor detection	RSD (%)	$KMnO_4$ titration	
1	94.27	5.12	97.36	−3.17
2	97.01	4.04	96.69	0.33
3	97.75	3.85	98.87	−1.13

[a] Relative error was the value of (Concentration $(H_2O_2)_{sensor}$ − Concentration $(H_2O_2)_{titration}$)/(Concentration $(H_2O_2)_{titration}$).

with the prepared chemical sensor. The results indicated that it was feasible to apply the proposed sensor to determine H_2O_2 in real samples.

4. Conclusions

In summary, a nonenzymatic chemical sensor based on $(PDDA\text{-}G/Fe_3O_4)_5$ multilayer films was fabricated with layer-by-layer assembly of negatively charged Fe_3O_4 NPs and positively charged PDDA-G through the electrostatic interaction on the ITO electrode to detect H_2O_2. Compared with enzyme-based biosensor, the applications of graphene and Fe_3O_4 NPs exhibited many advantages such as low cost, environmental friendliness and sustainable electrocatalytical activity. The increased current response was due to the synergistic effect of the excellent catalytic ability of Fe_3O_4 NPs and the good electric conductivity of graphene sheet. Moreover, the prepared chemical sensor exhibited a wide linear concentration range from 20 μM to 6.25 mM, a low detection limit (2.5 μM) and good stability for determination of H_2O_2. The application of the chemical sensor was evaluated by the determination of H_2O_2 in toothpaste, and satisfactory results were obtained.

Acknowledgements

This work was supported by the National Natural Science Foundation of China (no. 20890022), the National Key Basic Research Development Project of China (no. 2010CB933602) and (no. 2007CB714500).

Appendix A. Supplementary data

Supplementary data associated with this article can be found, in the online version, at doi:10.1016/j.talanta.2011.10.004.

References

[1] K.S. Novoselov, A.K. Geim, S.V. Morozov, D. Jiang, Y. Zhang, S.V. Dubonos, I.V. Grigorieva, A.A. Firsov, Science 306 (2004) 666–669.
[2] A.K. Geim, K.S. Novoselov, Nat. Mater. 6 (2007) 183–191.
[3] K.I. Bolotin, K.J. Sikes, Z. Jiang, M. Klima, G. Fudenberg, J. Hone, P. Kim, H. Stormer, Solid State Commun. 146 (2008) 351–355.
[4] M.D. Stoller, S.J. Park, Y.W. Zhu, J.H. An, R.S. Ruoff, Nano Lett. 8 (2008) 3498–3502.
[5] Y.W. Zhu, S. Murali, M.D. Stoller, K.J. Ganesh, W.W. Cai, P.J. Ferreira, A. Pirkle, R.M. Wallace, K.A. Cychosz, M. Thommes, D. Su, E.A. Stach, R.S. Ruoff, Science 332 (2011) 1537–1541.
[6] S. Wang, P.K. Ang, Z. Wang, A.L.L. Tang, J.T.L. Thong, K.P. Loh, Nano Lett. 10 (2010) 92–98.
[7] H.L. Li, S.P. Pang, S. Wu, X.L. Feng, K. Müllen, C. Bubeck, J. Am. Chem. Soc. 133 (2011) 9423–9429.
[8] T. Ramanathan, A.A. Abdala, S. Stankovich, D.A. Dikin, M. Herrera-Alonso, R.D. Piner, D.H. Adamson, H.C. Schniepp, X. Chen, R.S. Ruoff, S.T. Nguyen, I.A. Aksay, R.K. Prud'Homme, L.C. Brinson, Nat. Nanotechnol. 3 (2008) 327–331.
[9] S. Stankovich, D.A. Dikin, G.H.B. Dommett, K.M. Kohlhaas, E.J. Zimney, E.A. Stach, R.D. Piner, S.T. Nguyen, R.S. Ruoff, Nature 442 (2006) 282–286.
[10] H. Wu, J. Wang, X.H. Kang, C.M. Wang, D.H. Wang, J. Liu, I.A. Aksay, Y.H. Lin, Talanta 80 (2009) 403–406.
[11] Q. Lu, X.C. Dong, L.J. Li, X. Hu, Talanta 82 (2010) 1344–1348.
[12] M. Segal, Nat. Nanotechnol. 4 (2009) 612–614.
[13] K.S. Kim, Y. Zhao, H. Jang, S.Y. Lee, J.M. Kim, K.S. Kim, J.H. Ahn, P. Kim, J.Y. Choi, B.H. Hong, Nature 457 (2009) 706–710.
[14] C. Nethravathi, M. Rajamathi, Carbon 46 (2008) 1994–1998.
[15] C. Berger, Z.M. Song, X.B. Li, X.S. Wu, N. Brown, C. Naud, D. Mayou, T.B. Li, J. Hass, A.N. Marchenkov, E.H. Conrad, P.N. First, W.A. de Heer, Science 312 (2006) 1191–1196.
[16] X.B. Fan, W.C. Peng, Y. Li, X.Y. Li, S.L. Wang, G.L. Zhang, F.B. Zhang, Adv. Mater. 20 (2008) 4490–4493.
[17] J.L. Zhang, H.J. Yang, G.X. Shen, P. Cheng, J.Y. Zhang, S.W. Guo, Chem. Commun. 46 (2010) 1112–1114.
[18] Y.X. Xu, H. Bai, G.W. Lu, C. Li, G.C. Shi, J. Am. Chem. Soc. 130 (2008) 5856–5857.
[19] S. Zhang, Y.Y. Shao, H.G. Liao, M.H. Engelhard, G.P. Yin, Y.H. Lin, ACS Nano 5 (2011) 1785–1791.
[20] W.R. Yang, K.R. Ratinac, S.P. Ringer, P. Thordarson, J.J. Gooding, F. Braet, Angew. Chem. Int. Ed. 49 (2010) 2114–2138.
[21] J.F. Shen, Y.Z. Hu, C. Li, C. Qin, M. Shi, M.X. Ye, Langmuir 25 (2009) 6122–6128.
[22] C.Z. Zhu, S.J. Guo, Y.M. Zhai, S.J. Dong, Langmuir 26 (2010) 7614–7618.
[23] H. Deng, X.L. Li, Q. Peng, X. Wang, J.P. Chen, Y.D. Li, Angew. Chem. Int. Ed. 44 (2005) 2782–2785.
[24] L.Z. Gao, J. Zhuang, L. Nie, J.B. Zhang, Y. Zhang, N. Gu, T.H. Wang, J. Feng, D.L. Yang, S. Perrett, X.Y. Yan, Nat. Nanotechnol. 2 (2007) 577–583.
[25] L. Wang, E.K. Wang, Electrochem. Commun. 6 (2004) 225–229.
[26] C. Matsubara, N. Kawamoto, K. Takamura, Analyst 117 (1992) 1781–1784.
[27] A.I. Vogel, Textbook of Quantitative Chemical Analysis, Longman, U.K., 1989.
[28] Y.P. He, Q.L. Sheng, J.B. Zheng, M.Z. Wang, B. Liu, Electrochim. Acta 56 (2011) 2471–2476.
[29] E.E. Ferapontova, Electroanalysis 16 (2004) 1101–1112.
[30] K.F. Zhou, Y.H. Zhu, X.L. Yang, C.Z. Li, Electroanalysis 23 (2011) 862–869.
[31] N.I. Kovtyukhova, P.J. Ollivier, B.R. Martin, T.E. Mallouk, S.A. Chizhik, E.V. Buzaneva, A.D. Gorchinskiy, Chem. Mater. 11 (1999) 771–778.
[32] W.S. Hummers, R.E. Offeman, J. Am. Chem. Soc. 80 (1958) 1339.
[33] R. Massart, IEEE Trans. Magn. 17 (1981) 1247–1248.
[34] S.Y. Wang, X. Wang, S.P. Jiang, Phys. Chem. Chem. Phys. 13 (2011) 6883–6891.
[35] S. Stankovich, D.A. Dikin, R.D. Piner, K.A. Kohlhaas, A. Kleinhammes, Y.Y. Jia, Y. Wu, S.T. Nguyen, R.S. Ruoff, Carbon 45 (2007) 1558–1565.
[36] C.Z. Zhu, S.J. Guo, Y.X. Fang, S.J. Dong, ACS Nano 4 (2010) 2429–2437.
[37] D. Li, M.B. Müller, S. Gilje, R.B. Kaner, G.G. Wallace, Nat. Nanotechnol. 3 (2008) 101–105.
[38] V.C. Tung, M.J. Allen, Y. Yang, R.B. Kaner, Nat. Nanotechnol. 4 (2009) 25–29.
[39] M.A. Correa-Duarte, M. Grzelczak, V. Salgueiriño-Maceira, M. Giersig, L.M. Liz-Marzán, M. Farle, K. Sierazdki, R. Diaz, J. Phys. Chem. B 109 (2005) 19060–19063.
[40] L.H. Zhang, Y.M. Zhai, N. Gao, D. Wen, S.J. Dong, Electrochem. Commun. 10 (2008) 1524–1526.
[41] L.M. Li, Z.F. Du, S. Liu, Q.Y. Hao, Y.G. Wang, Q.H. Li, T.H. Wang, Talanta 82 (2010) 1637–1641.
[42] C.S. Shan, H.F. Yang, D.X. Han, Q.X. Zhang, A. Ivaska, L. Niu, Biosens. Bioelectron. 25 (2010) 1070–1074.
[43] X. Chen, C.C. Li, Y.L. Liu, Z.F. Du, S.J. Xu, L.M. Li, M. Zhang, T.H. Wang, Talanta 77 (2008) 37–41.
[44] M. ElKaoutit, I. Naranjo-Rodriguez, M. Domínguez, M.P. Hernández-Artiga, D. Bellido-Milla, J.L. Hidalgo-Hidalgo de Cisneros, Electrochim. Acta 53 (2008) 7131–7137.
[45] S.J. Yao, S. Yuan, J.H. Xu, Y. wang, J.L. Luo, S.S. Hu, Appl. Clay Sci. 33 (2006) 35–42.